Operation Enhancement of Permanent Magnet Excited Motors with Advanced Rotor Cooling System

Benedikt Groschup, Maxim Komissarov, Svetomir Stevic, Kay Hameyer

Institute of Electrical Machines (IEM), RWTH Aachen University
Schinkelstr. 4, D 52062 Aachen, Germany
e-mail: benedikt.groschup@iem.rwth-aachen.de

***Abstract*-Heat dissipation determines the power density of electric motor drives. This paper discusses the influence of different rotor and stator cooling approaches to extend the operational limits of permanent magnet synchronous motors for automotive application. A thermal lumped parameter model as well as an electromagnetic finite element model of the traction drive are employed. The thermal model is parameterized utilizing test bench measurements. The enhancement of advanced cooling approaches on operational limits is compared i.e. application of phase change material, heat pipes, air gap cooling, direct lamination cooling, shaft cooling and direct winding head cooling.**

I. Introduction

Due to the request of high power density and high efficiency, permanent magnet synchronous motors (PMSM) with rare earth permanent magnets are a commonly used motor topology for automotive traction applications. To avoid early winding failure or irreversible magnet degaussing, the maximum temperatures of the stator insulation system and the permanent magnets are limited [1, 2]. Several cooling methodologies can be found in literature, as shown in [3].

In this paper, different cooling approaches of PMSM are electromagnetically and thermally simulated and evaluated, with the objective to improve the operational range of the machine. In the low speed region of the PMSM, the most significant share of losses occurs in the stator winding and the operational range is limited by the maximum stator temperature. For high rotational speeds and electric basic frequencies, significant share of losses occurs in the stator and rotor lamination, resulting in high temperatures of the permanent magnets. In this work, six rotor-cooling and two stator-cooling concepts are discussed.

II. Loss Calculation Methodology

The data sheet of the studied permanent magnet synchronous motor is specified in Table I. This machine represents a state-of-the-art design for automotive traction application. The methodology utilized for electromagnetic finite element method (FEM) simulation of the entire motor torque-speed-map has been introduced in [4].

TABLE I
TECHNICAL DATA OF THE STUDIED PMSM

Specification	Value	
Number of pole pairs	p	6
Stator inner diameter	d_{stat}	180 mm
Peak torque	T_{peak}	250 Nm
Peak power	P_{peak}	125 kW
Axial length of rotor	l_{axial}	131 mm
Maximum electrical basic frequency	$f_{\mathrm{el,max}}$	1200 Hz

The iron losses for the rotor and stator are calculated based on the IEM iron loss formula, as shown in [4]. The magnet temperature T_{ma} influences the electric machine performance, as shown in [2]. In this study, the impact is considered for the remanence flux density $B_{\mathrm{r}}(T_{\mathrm{ma}})$ of the rare earth magnets with:

$$B_{\mathrm{r}}(T_{\mathrm{ma}}) = B_{r,0} \cdot \left(1 + \alpha_{\mathrm{NdFeB}} \cdot \left(T_{\mathrm{ma}} - T_{\mathrm{ma,0}}\right)\right). \quad (1)$$

The remanence flux density $B_{\mathrm{r,0}}$ is assumed to be 1.275 T at the temperature $T_{\mathrm{ma,0}}$ of 20 °C. The temperature coefficient α_{NdFeB} is assumed to be -0.1 %/K. The electromagnetic FEM simulation is calculated with flux densities, spanning from 1.1 T, corresponding to a temperature of 157.7 °C, in steps of 0.025 T, up to 1.275 T at $T_{\mathrm{ma,0}}$. The influence of the temperature on the dc copper losses is considered using the formula

$$P_{\mathrm{co}}(T_{\mathrm{wind}}) = P_{\mathrm{co,0}} \cdot \left(1 + \alpha_{\mathrm{co}} \cdot \left(T_{\mathrm{wind}} - T_{\mathrm{wind,0}}\right)\right), \quad (2)$$

with the calculated dc losses $P_{\mathrm{co,0}}$ for each operating point at the reference temperature $T_{\mathrm{wind,0}}$ of 60 °C and a temperature coefficient of copper α_{co} of 0.393 %/K. Using the same formula, the electric resistance for soft magnetic material in the stator and in the rotor increases with rising temperature, corresponding to the temperature coefficient of α_{Fe} of 0.5 %/K. The electric resistance is utilized in the calculation of the eddy current losses; thus, iron losses decrease with rising soft magnetic material temperature.

978-1-5386-9310-0/19/$31.00 ©2019 European Union

III. Thermal Lumped Parameter Model

For the thermal evaluation of an electrical machine, analytical as well as numerical methods are available. The analytical method comprises the lumped parameter thermal network LPTN. Bodies or parts of bodies i.e. parts of the electrical machine that exhibit thermal capacities and transitions to neighboring nodes are concentrated. The finite element method and the computational fluid dynamics (CFD) belong to the numerical methods. A detailed description of the mentioned approaches above is given in [5]. In this study, a simulation methodology to investigate several rotor and stator cooling concepts, as depicted in Table II, has to be selected. Therefore, the LPTN approach, as introduced in [6], is selected, showing the most appropriate compromise between accuracy and simulation and modeling effort.

The thermal reference cooling concept V00 is equipped with a helix-shaped stator housing jacket cooling and no rotor cooling. The used cooling fluid is water ethylene glycol mixture of 50/50 with an inlet volume flow of $10\,\mathrm{l/min}$ and an inlet temperature of $25\,°\mathrm{C}$. The used geometries of the studied cooling methodologies are shown in the cross-sectional view of the motor in Fig. 1. The direct winding cooling concept requires an enclosed end winding space which is filled with the cooling fluid. The fluid is transported via housing to the other end winding space.

TABLE II
OVERVIEW OF STUDIED ROTOR AND STATOR COOLING CONCEPTS

Cooling Concept	VS0: Stator housing cooling	VS1: Stator direct winding cooling
VR0: No rotor cooling concept	V00	V10
VR1: Rotor Lamination cooling	V01	V11
VR2: Rotor hollow shaft cooling	V02	V12
VR3: Rotor heat pipes	V03	V13
VR4: Rotor airgap cooling	V04	V14
VR5: Rotor phase change material	V05	V15

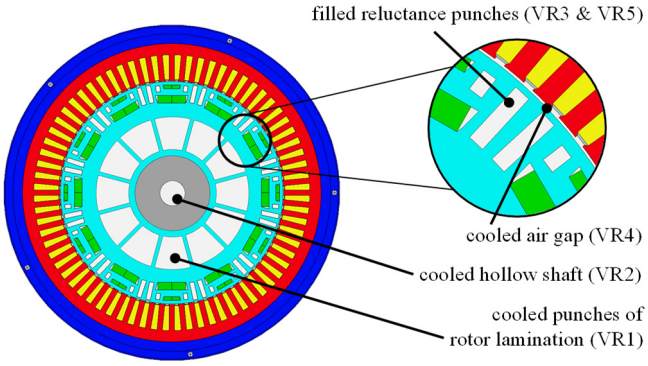

Fig. 1: Cross section of geometries for studied rotor cooling concepts.

The setup of the resistances for the cooling methodologies is crucial for a proper simulation. The cooling concepts are modeled by using the equations (3) to (7):

$$C_{\mathrm{th}} = c_{\mathrm{th}} \cdot m, \tag{3}$$

$$R_{\lambda} = \frac{l}{\lambda \cdot A} \text{ for conduction,} \tag{4}$$

$$R_{\mathrm{h}} = \frac{1}{h \cdot A} \text{ for convection,} \tag{5}$$

$$R_{\mathrm{h_r}} = \frac{1}{h_{\mathrm{r}} \cdot A} \text{ for radiation,} \tag{6}$$

$$R_{\mathrm{Fl}} = \frac{1}{\dot{V} \cdot \rho \cdot c_{\mathrm{th}}} \text{ within fluid.} \tag{7}$$

The thermal capacity Cth of the nodes is obtained from the specific thermal capacity c_{th} of the cooling fluid and its mass m within the channels. The thermal resistance caused by conduction to adjacent nodes is calculated with the equation (4), whereat k is the thermal conductivity of the material and A is the cross-sectional, respectively the transition area. The thermal transitions from the fluid to the adjacent nodes in case of convectional heat transfer i.e. the shaft or the rotor lamination are determined with equation (5). The thermal resistance for radiation (6) using the radiation exchange coefficient h_r is neglected due to relatively small temperatures. The fluid in flowing direction is modeled with equation (7).

The determination of the heat transfer coefficients h_{i} of the studied cooling concepts is crucial for the accuracy and the precision of the results. The value of the heat transfer coefficient h is calculated with

$$h = Nu \cdot \frac{k_{\mathrm{Fl}}}{l_{\mathrm{th}}}, \tag{8}$$

where Nu is the Nusselt number, k_{Fl} is the thermal conductivity of the fluid and l_{th} is the characteristic length of the thermal problem. The characteristic length of the thermal problem is calculated in dependency of different geometrical setups, as depicted in Fig. 2.

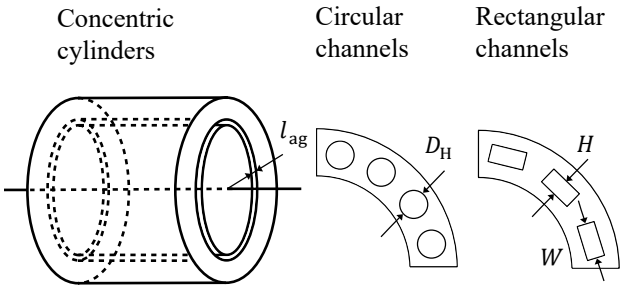

Fig. 2: Geometry arrangements for the calculation of heat transfer coefficient.

978-1-5386-9310-0/19/$31.00 ©2019 European Union

The characteristic length l_{th} for cooling channels of round or rectangular shape is also referred to as the hydraulic diameter D_{h}. The following formula is used for calcualtion.

$$l_{\mathrm{th}} = D_{\mathrm{h}} = 4 \cdot \frac{A_{\mathrm{channel}}}{C_{\mathrm{channel}}} \quad \text{for channels} \tag{9}$$

$$l_{\mathrm{th}} = 2 \cdot l_{\mathrm{ag}} \quad \text{for concentric cylinders} \tag{10}$$

The air gap length l_{ag}, the cross-sectional area A_{channel} and the circumference C_{channel} of the channel are considered. It has to be noted that in literature [7], the factor two in the air gap correlation misses, because the formula is then correlated to the heat transfer of either rotor or stator surface area to the air gap and not from the rotor to the stator surface area. Two additional dimensionless numbers that are used for calculation of the Nusselt number *Nu* are needed, i.e. the Reynolds number *Re* and the Prandtl number *Pr*. The Reynolds describes the ratio between the inertial forces to viscous forces

$$Re = D_{\mathrm{h}} \cdot \frac{v_{\mathrm{fl}}}{\nu}, \tag{11}$$

where v_{fl} is the flow velocity and ν is the kinematic viscosity of the fluid. The Prandtl number *Pr* describes the ratio between the kinematic viscosity ν and the thermal diffusivity and is determined with the following equation:

$$Pr = \frac{\nu \rho c_{\mathrm{p}}}{k}, \tag{12}$$

where ρ is the fluid density and c_{p} is the specific heat capacity. For all cooling technologies with forced flow of a liquid cooling medium (VR1, VR2, VS0, VS1) a water ethylene glycol mixture of 50/50 is used. The Prandtl number of the fluid is assumed to be 30.26 at inlet temperature [8]. The flow is fully laminar at $Re < 2300$ for round and rectangular channels and at $Re < 2800$ for the air gap correlation. In the event of exceeding 3000 the fluid flow is assumed to be turbulent. In each flow condition, the determination of the Nusselt number is carried out differently. The equations (13) to (15) present calculations of the Nusselt number at laminar flow in concentric cylinders (13), circular channels (14) and rectangular channels (15) [9].

$$Nu = 7.54 + \frac{0.03 \cdot \frac{l_{\mathrm{th}}}{L} \cdot Re \cdot Pr}{1 + 0.016 \cdot \left(\frac{l_{\mathrm{th}}}{L} \cdot Re \cdot Pr\right)^{2/3}} \tag{13}$$

$$Nu = 3.66 + \frac{0.065 \cdot \frac{l_{\mathrm{th}}}{L} \cdot Re \cdot Pr}{1 + 0.04 \cdot \left(\frac{l_{\mathrm{th}}}{L} \cdot Re \cdot Pr\right)^{2/3}} \tag{14}$$

$$Nu = 7.49 - f\left(\frac{H}{W}\right) + \frac{0.065 \cdot \frac{l_{\mathrm{th}}}{L} \cdot Re \cdot Pr}{1 + 0.04 \cdot \left(\frac{l_{\mathrm{th}}}{L} \cdot Re \cdot Pr\right)^{2/3}} \tag{15}$$

Several equations for the Nusselt correlations can be found in literature. As an example, the formula (14) describes a flow condition of a thermal developing and hydrodynamic developed flow. The assumption of hydrodynamic developed flow is applicable after the length $L_{\mathrm{th}}(5\%)$ of

$$\frac{L_{\mathrm{th}}(5\%)}{D_{\mathrm{h}}} = 0.033\, Re\, Pr, \tag{16}$$

as stated in [10]. The results of this correlation are in coincidence with formula presented for the use of thermal developing and hydrodynamic developing flow for small values of $Re \cdot Pr \cdot D_{\mathrm{h}}/L$. For both cases, the asymptote is 3.66. For higher values $Re \cdot Pr \cdot D_{\mathrm{h}}/L$, the values of the resulting *Nu* numbers defer with a maximum at the start of the transition area to turbulent flow. Moreover, an additional geometry factor is implemented that depends on the height *H* and the width *W* of the cooling channels [9].

$$f\left(\frac{H}{W}\right) = 17.02 \cdot \frac{H}{W} - 22.43 \cdot \left(\frac{H}{W}\right)^2 + 9.94 \cdot \left(\frac{H}{W}\right)^3 \tag{17}$$

In the case of a turbulent fluid flow, the calculation of the Nusselt number is carried out with the following equation [11]:

$$Nu = \frac{f}{8} \cdot \frac{(Re - 1000) \cdot Pr}{1 + 12.7 \cdot \left(\frac{f}{8}\right)^{\frac{1}{2}} \cdot \left(Pr^{\frac{2}{3}} - 1\right)}, \tag{18}$$

whereat an additional friction factor *f* for smooth walls is used.

$$f = [0.79 \cdot \ln(Re) - 1.64]^{-2} \tag{19}$$

The heat transfer correlation in the air gap is based on calculations and measurements introduced in [8] and [12]. The Taylor number Ta describes the flow conditions in the air gap. In the present study the formula introduced in [13] is utilized

$$Ta = \frac{\rho \omega r_{\mathrm{rot}}^{0.5} l_{\mathrm{ag}}^{1.5}}{\mu}, \tag{20}$$

with the rotational velocity ω, the outer radius of the rotor r_{rot}, and the dynamic viscosity of the fluid μ. In other literature, different definitions of the Taylor number can be found. In [14], the squared value of the definition as shown in (20) is used and called modified Taylor number Ta_{m}. In case of no axial flow through the airgap, the following formula for the calculation of the Nusselt number is used [6].

$$Nu = \begin{cases} 2 & \text{for } Ta < 41 \\ 0.212\, Ta^{0.63}\, Pr^{0.27} & \text{for } 41 \leq Ta \leq 100 \\ 0.386\, Ta^{0.5}\, Pr^{0.27} & \text{for } 100 \leq Ta \end{cases} \tag{21}$$

In addition to the Taylor vortices caused by rotation, an axial airflow in the air gap is added in VR4. The axial Reynolds

978-1-5386-9310-0/19/$31.00 ©2019 European Union

number Re_{ax} is introduced and used for the description of the axial flow, whereby the radial flow is described by the Taylor number Ta. Some of the first investigations of axial flow with rotation were done by [12]. In following studies like [13] different flow regions were determined with different Nusselt correlations in dependency of both, the Taylor number Ta and the axial Reynolds number Re_{ax}. With increasing axial Reynolds number Re_{ax}, the region of laminar flow ($Nu = 2$) in the airgap is expanded to higher Taylor numbers Ta. [14]. A summary of the assumptions that are used in the present study is given in [15].

For the heat pipe model VR3, the reluctance punches are filled with a copper water heat pipe to reduce the axial temperature coefficient within the machine. For the wall and the wick, a thickness of 0.6 mm and 0.3 mm respectively are selected based on the design as shown in [16]. For the thermal conductivity of the wall, 300 W/mK representing copper and for the wick 200 W/mK as given in [17] is used. The axial conductivity of the wick and the wall are neglected. The thermal conductivity of the fluid is assumed to be 100000 W/mK as an average value given in [18]. The total resistance of two walls, two wicks and the fluid results in 1.59 mK/W.

The usage of PCM in VR5 is intended to reduce the increase of rotor temperature in transient operation. The phase transition occurs between 80 °C and 82 °C and leads to a consumption of latent heat of 250 kJ/kg [19]. The total mass of PCM is $m_{PCM} = 86.3$ mg. The maximum energy that can be dissipated is 21.6 J. The thermal capacity of the rotor magnets and the rotor lamination is 60.4 J/K, which means that less energy is required for the phase transition of PCM when compared to heating up the rotor for one degree Celsius.

IV. Measurement Setup and Parameterization

In order to get a suitable accuracy for the further study, the thermal model of the reference design V00 is parameterized, using test bench measurements of the electric motor, as depicted in Fig. 3. The test machine is driven on an axle test bench with two load machines and a differential.

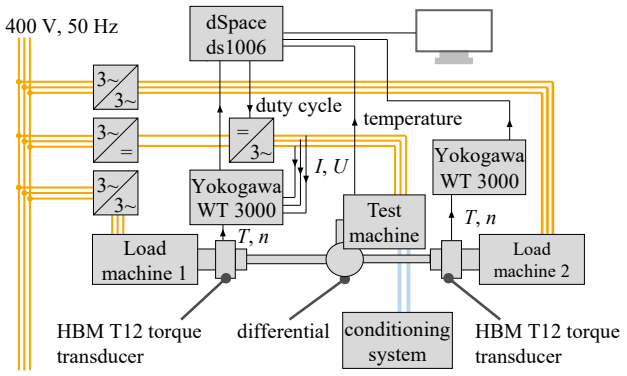

Fig. 3: Measurement setup of the thermal characterization.

TABLE III
MEASURED OPERATING POINTS

Operating Point	Speed	Torque
OP1, OP2, OP3	1000 rpm	50 Nm, 125 *Nm*, 200 *Nm*
OP4, OP5, OP6	3000 rpm	50 Nm, 125 *Nm*, 200 *Nm*
OP7, OP8	5000 rpm	75 Nm, 125 Nm
OP9	7000 rpm	50 Nm
OP10	9000 rpm	50 Nm
OP11	10000 rpm	50 Nm
OP12	11000 rpm	40 Nm

The transient temperature of the end winding of the machine for a total of 12 different operating points that are shown in Table I is measured. The initial temperature of the machine is set to 25 °C and the machine runs at each selected operating point for 30 min. After completing this operation, the motor was stopped and cooled down to the ambient temperature.

The test bench measurements are used to parameterize the developed LPTN model of V00. The values of the heat transmission coefficient of the housing to the stator cooling fluid h_{col}, the thickness of the insulation material in the stator notches d_{iso} and the air gap between the stator stack and the housing d_{air} are not exactly known. The three parameters show a significant impact on the temperature characteristics and are used for the parameterization of the LPTN until the differences in comparison to the measurement are below 5 K. There are several approaches to solve the optimization problem, as described in [20]. In this study, a manual adaptation of the three above mentioned parameters leads to a sufficient match of measurement and simulation results and thus no optimization algorithm needs to be used. Both, the boundary conditions and the results of the parameterization are shown in Table IV.

TABLE IV
PARAMETERIZATION RESULTS

Parameter	Lower Boundary	Upper Boundary	Result
h_{col} in W/m²K	800	1600	1400
d_{iso} in mm	0.2	0.3	0.27
d_{air} in mm	0.005	0.05	0.021

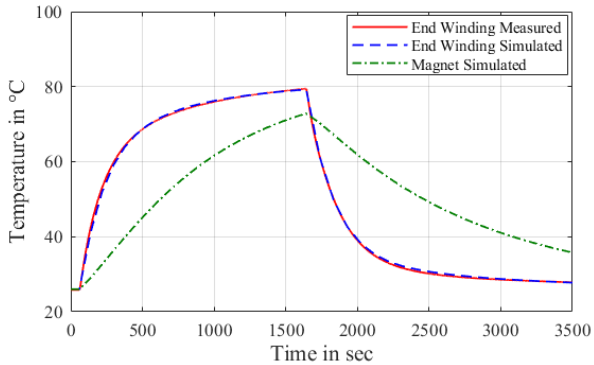

Fig. 4: Comparison of measured and simulated end-winding temperature after parameterization.

978-1-5386-9310-0/19/$31.00 ©2019 European Union

The simulated and measured end winding temperatures are illustrated in Fig. 4 for operating point OP8 with 5000 rpm and 125 Nm. The maximum absolute difference between the temperatures obtained from the simulation and measurement in this operating point is 0.6°C at the time stamp of 2400 s, resulting in the maximum relative difference of 1.9 %.

V. Results

The effectivity of the design with PCM (V05 and V15) has to be evaluated in transient operation, as no significant influence on heat transmission coefficient is added to the model. Due to the small mass of PCM that is added to the rotor, the design shows no significant delay in the temperature rise and is not capable of increasing the short term operating range of the motor, as shown in Fig. 5. In order to obtain notable changes in the rotor heating process, a more significant mass of PCM has to be added to the model.

In order to identify the enhancement of the rotor cooling concepts, in reference to the model without rotor cooling V00, the operational limits for continuous operation are determined and shown in Fig. 6 and Fig. 7. The maximum steady state temperatures of the motor are set to 120 °C for the permanent magnets and 180 °C for the winding insulation system.

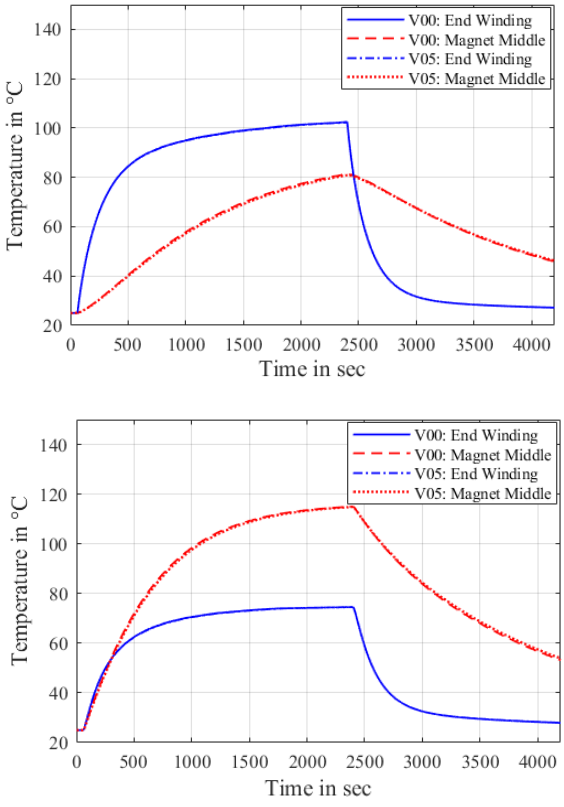

Fig. 5: Influence of phase change material V05 in comparison to baseline V00 for 200 Nm, 3000 rpm (top) and 40 Nm, 12000 rpm (bottom).

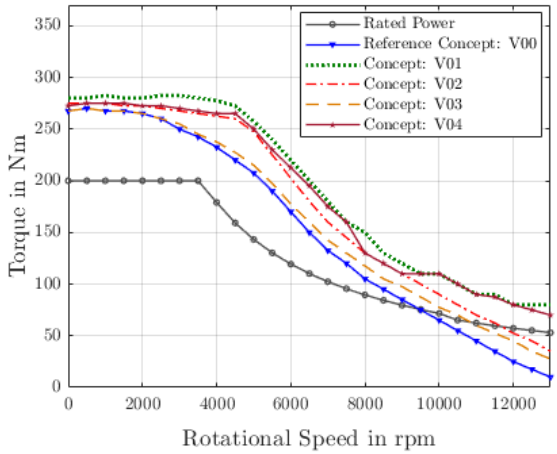

Fig. 6: Continuous operational limits of different rotor cooling technologies.

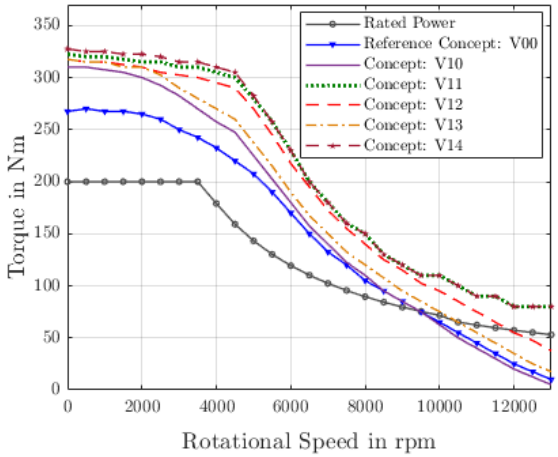

Fig. 7: Continuous operational limits of different rotor and stator cooling technologies.

In Fig. 6, the cooling concepts for the rotor V01, V02, V03, V04 are compared to the reference model V00. The highest improvement of the operational limits is provided by the rotor lamination cooling, followed by the hollow shaft cooling, airgap cooling and the heat pipes. The influence of the heat dissipation from the rotor and therefore from the magnets becomes apparent above 2000 rpm, where the maximum permissible magnet temperatures are restrictive. At a speed of 7000 rpm, the continuous power is enhanced by 35% with the rotor lamination cooling concept V01, by 31.6% with airgap cooling concept V04, by 20% with a rotor hollow shaft cooling concept V02 and by 7.5% with the rotor heat pipes V03 compared to the baseline without rotor cooling V00.

In Fig. 7, the above discussed cooling concepts are combined with an additional direct end winding cooling. The concept V10 depicts the reference model with direct end winding cooling. The effectivity of the heat dissipation is noticeable at speeds below 7000 rpm. At a speed of 1000 rpm, the continuous power is increased by 21.3% with concept V14, by 19.5% with concept V11, by 17.5% with V12 as well as with V13 and by 15% with V10 compared to the baseline V00.

978-1-5386-9310-0/19/$31.00 ©2019 European Union

VI. CONCLUSIONS AND FUTURE WORK

The direct rotor lamination cooling concept V01 provides the best result, referring to the increase of operational limits in the field weakening area, in which the maximum permissible magnet temperature restricts the operational range of the PMSM. With this approach, the continuous operation power can be increased by 35% at a speed of 7000 rpm. The usage of heat pipes increases the operational limit at 7000 rpm by 7.5 % with no additional pump or pipe system needed. Furthermore, the system leads to a decreased axial temperature difference in the motor and thus is effective for machines with large axial length. The direct end winding cooling concept exhibits a significant enhancement of the operational limits in the base speed area, in which the maximum permissible temperatures of the end winding limit the operational range. Hence, the continuous power is increased by 18% at a speed of 1000 rpm without any additional rotor cooling.

REFERENCES

[1] M. Jaeger, A. Ruf, K. Hameyer, and T. G.-v. Tongeln, "Thermal Analysis of an Electrical Traction Motor with an Air Cooled Rotor," in *IEEE Transportation and Electrification Conference and Expo (ITEC): Long Beach, California, June 13-15, 2018*, Long Beach, CA, USA, 2018, pp. 467–470.

[2] S. Ruoho, J. Kolehmainen, J. Ikaheimo, and A. Arkkio, "Interdependence of Demagnetization, Loading, and Temperature Rise in a Permanent-Magnet Synchronous Motor," *IEEE Trans. Magn.*, vol. 46, no. 3, pp. 949–953, 2010.

[3] M. Popescu, D. A. Staton, A. Boglietti, A. Cavagnino, D. Hawkins, and J. Goss, "Modern Heat Extraction Systems for Power Traction Machines—A Review," *IEEE Trans. on Ind. Applicat.*, vol. 52, no. 3, pp. 2167–2175, 2016.

[4] N. Leuning, S. Elfgen, B. Groschup, G. Bavendiek, S. Steentjes, and K. Hameyer, "Advanced Soft- and Hard-Magnetic Material Models for the Numerical Simulation of Electrical Machines," *IEEE Trans. Magn.*, vol. 54, no. 11, pp. 1–8, 2018.

[5] A. Boglietti, A. Cavagnino, D. Staton, M. Shanel, M. Mueller, and C. Mejuto, "Evolution and Modern Approaches for Thermal Analysis of Electrical Machines," *IEEE Trans. Ind. Electron.*, vol. 56, no. 3, pp. 871–882, 2009.

[6] D. Staton, A. Boglietti, and A. Cavagnino, "Solving the More Difficult Aspects of Electric Motor Thermal Analysis in Small and Medium Size Industrial Induction Motors," *IEEE Trans. Energy Conver.*, vol. 20, no. 3, pp. 620–628, Sep. 2005.

[7] J. Pyrhönen, T. Jokinen, and V. Hrabovcová, Eds., *Design of Rotating Electrical Machines,* 1st ed. Chichester: Wiley, 2008.

[8] G. I. Taylor, "Distribution of Velocity and Temperature between Concentric Rotating Cylinders," *Proceedings of the Royal Society A: Mathematical, Physical and Engineering Sciences*, vol. 151, no. 874, pp. 494–512, 1935.

[9] A. F. Mills, *Heat transfer,* 2nd ed. Upper Saddle River, NJ: Prentice Hall, 1999.

[10] D. K. Edwards, V. E. Denny, and A. F. Mills, *Transfer Processes: An Introduction to Diffusion, Convection and Radiation,* 2nd ed. Washington D.C., London: McGraw-Hill, 1979.

[11] V. Gnielinski, "New Equations for Heat and Mass Transfer in Turbulent Pipe and Channel Flow," *International Chemical Engineering*, vol. 16, no. 2, pp. 359–368, 1976.

[12] C. Gazley, JR., "Heat-Transfer Characteristics of the Rotational and Axial Flow Between Concentric Cylinders," *Transactions of the ASME*, vol. 80, pp. 79–90, 1958.

[13] J. Kaye, "Modes of Adiabatic and Diabatic Fluid Flow in an Annulus with an Inner Rotating Cylinder," *Transactions of the ASME*, vol. 80, pp. 753–765, 1958.

[14] K. M. Becker and J. Kaye, "Measurements of Diabatic Flow in an Annulus with an Inner Rotating Cylinder," *J. Heat Transfer*, vol. 84, no. 2, pp. 97–104, 1962.

[15] Y. C. Chong, "Thermal Analysis and Air Flow Modelling of Electrical Machines," Ph.D. Dissertation, The University of Edinburgh, Edinburgh, 2015.

[16] Z. J. Zuo and A. Faghri, "A Network Thermodynamic Analysis of the Heat Pipe," *International Journal of Heat and Mass Transfer*, vol. 41, no. 11, pp. 1473–1484, 1998.

[17] M. T. Ababneh, F. M. Gerner, P. Chamarthy, P. de Bock, S. Chauhan, and T. Deng, "Thermal-Fluid Modeling for High Thermal Conductivity Heat Pipe Thermal Ground Planes," *Journal of Thermophysics and Heat Transfer*, vol. 28, no. 2, pp. 270–278, 2014.

[18] M. Bradford, "The Application of Heat Pipes to Cooling Rotating Electrical Machines," in *IEEE 4th International Conference on Electrical Machines and Drives*, London, UK, 1989, pp. 145–149.

[19] S. Wang, Y.-Z. Li, Y. Liu, H. Zhou, Y. Li, W. Guo, and X. Xiao, "Temperature Control of Permanent-Magnet Synchronous Motor Using Phase Change Material," in *IEEE International Conference on Advanced Intelligent Mechatronics (AIM)*, Busan, South Korea, 2015, pp. 1635–1640.

[20] G. Guedia Guemo, P. Chantrenne, and J. Jac, "Parameter Identification of a Lumped Parameter Thermal Model for a Permanent Magnet Synchronous Machine," in *IEEE International Electric Machines and Drives Conference*, Chicago, IL, USA, 2013, pp. 1316–1320.

978-1-5386-9310-0/19/$31.00 ©2019 European Union